

# A Design Methodology for Sensing-Ready Concentric Rings-Based Chipless RFID Tags With Effective Spectrum Use and High Coding Capacity

Nadeem Rather<sup>1</sup>, John L. Buckley<sup>1</sup>, Brendan O'Flynn<sup>1</sup>, *Senior Member, IEEE*, Melusine Pigeon,  
and Roy B. V. B. Simorangkir<sup>2</sup>, *Member, IEEE*

**Abstract**—This paper introduces an innovative strategy for the development of sensing-ready concentric rings-based chipless radio frequency identification (CRFID) tags. Our approach is marked by the novel use of exponentially increasing spacing, a significant departure from the conventional uniform spacing method. This innovative design results in an impressive 88.2% improvement in tag data encoding capacity compared to traditional designs. Importantly, our design framework not only advances the current state of CRFID tag technology but also methodically lays the foundation for future integration of high-resolution sensing capabilities. This is achieved by strategically utilizing the innermost ring as a prospective sensing site, complemented by the implementation of nulls for data encoding achieved through the addition of an extra ring at the tag's outermost edge. Notably, all these features represent advancements that have not been demonstrated in previously published concentric rings-based CRFID tags. To empirically validate our methodology, we have developed and tested 18-bit example tags optimized for operation within the ultrawideband (UWB) spectrum, covering a range from 3.1 to 10.6 GHz. The radar cross-section (RCS) response of these tags exhibits well-distributed resonances, culminating in a high encoding capacity of 17.65 bits/ $\lambda^2$ /GHz. Preliminary results using capacitors connected to the innermost ring underscore the future sensing potential of our tags, setting the stage for more advanced sensing implementations in subsequent research.

**Index Terms**—Chipless RFID tags, concentric resonators, circular rings, encoding capacity, radar cross section, sensing.

Manuscript received 22 September 2023; revised 1 November 2023 and 12 December 2023; accepted 1 January 2024. Date of publication 9 January 2024; date of current version 26 January 2024. This work was supported in part by the Science Foundation Ireland (SFI) as part of the SFI Centre VistaMilk under Grant SFI 16/RC/3835; in part by the CONNECT Centre for Future Networks and Communications under Grant 13/RC/2077; in part by the Insight Centre for Data Analytics under Grant SFI/12/RC/2289 and Grant 16/RC/3918-CONFIRM; in part by the Enterprise Ireland funded Holistics DTIF (Disruptive Technologies Innovation Fund) under Grant EI-DT20180291-A; and in part by the European Regional Development Fund. (Corresponding author: Nadeem Rather.)

Nadeem Rather, John L. Buckley, and Brendan O'Flynn are with the Wireless Sensor Network Group, Tyndall National Institute, University College Cork, Cork, T12 R5CP Ireland (e-mail: nadeem.rather@tyndall.ie).

Melusine Pigeon is with the Department of Electronic and Electrical Engineering, University of Bath, BA2 7AY Bath, U.K.

Roy B. V. B. Simorangkir is with the Department of Engineering, Durham University, DH1 3LE Durham, U.K.

Digital Object Identifier 10.1109/JRFID.2024.3351678

## I. INTRODUCTION

THE TOPOLOGY and arrangement of resonators play a critical role in achieving the desired frequency-selective reflection of a Radar Cross Section (RCS)-based Chipless Radio Frequency Identification (CRFID) tag. Hence, it becomes crucial to delve into and comprehend the diverse solutions available to meet specific application requirements, encompassing design effectiveness [1], robust signal processing [2], [3], improving encoding capacity [4], and spectrum efficiency [5], [6], as well as sensing capabilities [7], [8], [9]. For instance, in [10], [11], arrays of 20 and 10 C-shaped resonators, respectively, were employed to devise 20-bit and 10-bit capacity tags, respectively, emphasizing compactness with high encoding capacities. Furthermore, in [12], a tag featuring five C-shaped resonators was developed with both identification and sensing capability. Four of these resonators encoded binary data, while the fifth, enhanced with silicon nanowires, enabled temperature and humidity sensing. This amalgamation yielded a tag that resonated at the desired frequencies and demonstrated amplified sensitivity, making it suitable for environmental monitoring applications.

Similarly in [13], U and inverted-U-shaped slots-based tags were employed to improve data capacity and spectrum efficiency while retaining a low-profile design. The paper achieved a high 22-bit capacity tag within a 1.7 GHz bandwidth, emphasizing efficient spectrum utilization. In [14], U-shaped resonators were utilized to develop a robust CRFID tag for structural crack sensing applications. Despite the advancements, one critical limitation in the above-mentioned designs is their inherent sensitivity to the polarization of the interrogating antenna. This means that even a minor shift in tag orientation could lead to a decrease in backscatter signal strength, potentially resulting in reduced read ranges or undetectable signals. These challenges make these tags less practical for real-world applications. In response to these issues, several studies have proposed polarization-insensitive concentric strip/slot-rings configuration [15], [16], [17], [18], [19], [20], [21], [22], [23]. For example, in [15], [18] concentric square rings were employed to create compact 5-bit CRFID tags, with [18] focusing specifically on achieving polarization insensitivity. Additionally, various ring shapes, including circular [24], elliptical [17], triangular [16], pentagonal [19], and octagonal [25], have been explored in

the literature for developing compact, high data capacity, and orientation-insensitive concentric ring-based chipless RFID tags.

Apart from enabling a polarization-independent tag, such a nested configuration is also beneficial for increasing the bit capacity while retaining a low tag profile. The typical design strategy in the literature for such a tag is to have a constant spacing between adjacent rings, which may alternatively be seen as the radii of the rings varying linearly. In this configuration, each concentric ring within the tag is designed to resonate at a specific frequency, which can be associated with binary values, either '0' or '1', depending on the chosen design approach. To encode specific bit combinations onto the tag, designers have the flexibility to determine which rings should resonate and which should not. For instance, rings intended to represent a binary '1' remain unaltered, resonating at their designated frequency. In contrast, rings intended to represent a binary '0' undergo specific design modifications (detuning), to prevent resonance at the originally intended frequency, or removed altogether. This selective tuning or removal of rings forms the basis for encoding distinct bit combinations within the concentric strip/slot-rings configuration.

There is, however, a drawback to the constant rings spacing approach described above. Due to the inverse relationship between the ring's radius and resonant frequency, as approximated in [26], the linear variation in the radii of the rings results in an exponential distribution of the tag's resonances in the RCS response. Specifically, at lower frequencies, the distances between successive resonance peaks are narrow, but they widen exponentially as the frequency increases. An example to illustrate this can be seen in [19]. The developed tag exhibited resonance peaks distributed non-equally between 4 to 19 GHz, with 80% of the peaks (or the total encoded bits) occupying the first half of the spectrum and only 20% occupying the second half. A similar phenomenon can also be seen in [16], [17], [18], [20], [21], [22], [23], [25]. Such ineffective use of spectrum can be very problematic in the case of concentric rings tags with high encoding capacity, especially when the constraints of tag size and/or operating frequency compliance (e.g., Federal Communications Commission (FCC) rules on ultrawideband (UWB) communications [27]) are in place. As more bits are added to the tags, the resonance peaks representing these bits densely populate the lower frequency region. The close proximity of these resonance peaks can lead to overlaps, making it challenging to distinguish individual bits. Consequently, the decoding process becomes increasingly intricate, demanding more sophisticated signal processing algorithms [28], [29], [30], especially for bits concentrated in the lower frequency spectrum.

In this paper, a design strategy to solve the above problem is presented. Taking the implication of the inverse relationship between the radius and the resonant frequency of the ring, for the first time, the concept of exponentially increasing spacing for the development of concentric rings-based tags is demonstrated. Compared to the traditional design approach, the gradual change in the distance between consecutive rings, or equivalently the exponential change in the rings' radii, improves the resonance distribution of the tag. Not only does

this result in a more convenient decoding process, but we also show an increase in bit encoding capacity by 88.2% compared to the same-sized tag built using the constant spacing approach. Building upon the insights from our previous exploration in [31], we employ the concept of nulls, rather than resonance peaks, for data encoding. This modification is particularly instrumental in laying the groundwork for future sensing applications using the innermost ring of the tag. It is important to note that, in contrast to our previous study [31], this paper provides a comprehensive explanation of the design principle behind the exponential spacing technique, which is crucial for comprehending the proposed concept and its implementation. On top of that, a study comparing the RCS performance of the tags generated using the exponential and equal spacing techniques is presented to showcase the significance of the proposed method for attaining effective spectrum utilization and high coding capacity. Further, we demonstrate clearly how the proposed concept can be implemented in the development of polarization-insensitive tags for simultaneous identification and future sensing encoding. Finally, we present a systematic tag synthesis guideline and validate the proposed concept with proof-of-concept example tags that exhibit a higher bit capacity and spectrum efficiency than previously reported concentric rings/slots-based CRFID tags. All of this has not been covered in [31], which focuses solely on exploring the concept of adding an extra outermost ring to facilitate the use of RCS nulls for encoding.

As a proof of concept, the proposed approach is utilized to develop 18-bit concentric rings tags occupying the FCC-specified UWB band, 3.1 to 10.6 GHz. Our decision on the frequency range and the encoding capacity strikes a balance between regulatory compliance, adaptability to real-world applications, and practical fabrication constraints. The initial seventeen bits are primarily allocated for identification, serving to uniquely represent and classify each tag. Meanwhile, the final bit is designated as a platform for potential future sensing applications. To demonstrate the latter, different values of capacitors are integrated with the innermost ring, effectively mimicking the envisioned sensing mechanism involving materials with stimuli-sensitive permittivity. Validated by the measurements, the tag demonstrates an effective spectrum usage, with the eighteen bits well distributed within 3.45 to 9.4 GHz. The frequency position of the last bit, reserved for high-resolution sensing, can be varied within the remaining UWB spectrum, demonstrating the tag's potential for advanced sensing applications in future iterations.

## II. PROPOSED SOLUTION

### A. Tag Configuration

The proposed design is based on a circular ring resonator (CRR) topology in a nested configuration, as shown in Fig. 1. The circular shape is chosen for ease of analysis and construction. The tag comprises a number of one-wavelength circumference rings with a constant track width ( $t_w$ ) that represent  $N$ -bit data encoding capacity (i.e., 1 bit for sensing,  $N - 1$  bits for identification). The rings are printed on an ungrounded single-layer substrate with a thickness of  $h$ . The

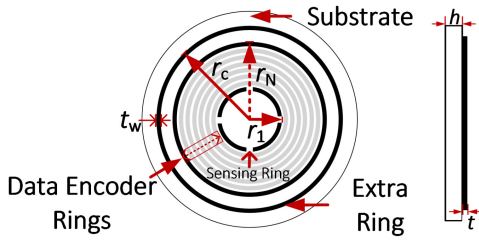


Fig. 1. Geometry of the proposed CRFID tag.

innermost ring is reserved for sensing; the outermost ring is added to enable the ‘null encoding’ and the rings in between are used for data identification. The most significant bit (MSB),  $b_1$ , is represented by the ring with radius  $r_N$  and the least significant bit (LSB),  $b_N$ , is represented by the ring with radius  $r_1$ . The key differences of the proposed design compared to the previously reported concentric rings tags are the inclusion of the extra ring and the exponential growth of the radii (i.e.,  $r_1$  to  $r_c$ ) of the composing rings from the inner to the outermost ring. The role of both techniques, as well as the synthesis of the tag, are explained in the next subsections. The EM simulations for investigating the tag design were performed using CST Microwave Studio 2022. Vertically-polarized plane waves were used to excite the tag, and an RCS probe was used to measure the RCS of the tag.

### B. Exponential Spacing

Given the circular ring resonator is electrically large, the relationship between its radius ( $r$ ) and resonant frequency ( $f_r$ ) can be approximated by [26]

$$f_r = c / (2\pi r \sqrt{\epsilon_{eff}}) \quad (1)$$

where  $c$  is the speed of light in the vacuum, and  $\epsilon_{eff}$  is the effective dielectric permittivity. From the inverse relationship between  $r$  and  $f_r$  in (1), it can be understood that for a tag comprised of multiple ring resonators, a linear progression of the rings’ radii leads to an exponential distribution of the tag resonant frequencies in the RCS response. This explains the previously noted issue with conventional concentric rings tags. It can also be inferred from (1) that if the radii of rings vary exponentially, the linear distribution of the tag resonant frequencies can be expected. Based on this, the concept of increasing the spacing between two successive rings exponentially, which translates into exponentially varying rings’ radii, is proposed to achieve a concentric rings tag with more optimal spectrum usage.

To illustrate the significance of this concept, three 10-bit concentric rings tags were developed (Fig. 2). The first tag (tag A) represents the standard design with constant spacing between the rings, whereas the second (tag B) and third tags (tag C) show the case when the exponential spacing technique is applied. For simplicity, air and PEC were used in simulations as the substrate and the conductor layers of all tags, respectively. The lower and upper operating frequency limits of the tags were defined at 2 and 11 GHz, respectively. Such a wide spectrum was set for ease of observation of the RCS response.

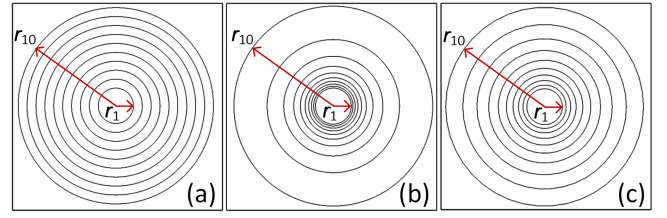


Fig. 2. 10-bit CRFID tags developed using (a) constant spacing (tag A), (b) exponential spacing 1 (tag B), and (c) exponential spacing 2 (tag C).

TABLE I  
CALCULATED RADII OF THE DEVELOPED TAGS IN FIG. 2

| Ring No. | Encoded Bit No. | Tag A $r$ (mm) | Tag B $r$ (mm) | Tag C $r$ (mm) |
|----------|-----------------|----------------|----------------|----------------|
| $r_1$    | $b_{10}$ (LSB)  | 4.34           | 4.34           | 4.34           |
| $r_2$    | $b_9$           | 6.51           | 4.77           | 5.24           |
| $r_3$    | $b_8$           | 8.68           | 5.30           | 6.33           |
| $r_4$    | $b_7$           | 10.84          | 5.96           | 7.65           |
| $r_5$    | $b_6$           | 13.01          | 6.81           | 9.25           |
| $r_6$    | $b_5$           | 15.18          | 7.95           | 11.18          |
| $r_7$    | $b_4$           | 17.35          | 9.54           | 13.51          |
| $r_8$    | $b_3$           | 19.52          | 11.93          | 16.33          |
| $r_9$    | $b_2$           | 21.69          | 15.91          | 19.74          |
| $r_{10}$ | $b_1$ (MSB)     | 23.86          | 23.86          | 23.86          |

For all three tags, the radii of the outer and innermost rings were firstly determined by correlating them with the specified lower and upper-frequency limits, respectively, using (1). As a result, the radii of the largest and smallest rings of the three tags are identical. For tag A, the remaining eight rings were added between the inner and outermost rings while keeping a constant gap of 2.17 mm between each pair of rings. For tag B, on the other hand, the radii of the remaining eight rings were calculated with (1), associating them with equally spaced frequency points within the frequency limits (i.e.,  $f_r = 3, 4, 5, \dots, 10$  GHz). In contrast to tag B, for tag C a growth rate ( $g_r$ ) was established, by which factor the radii of the remaining eight rings were varied according to the following equation

$$r_n = r_1(1 + g_r)^{n-1}, n \geq 2 \quad (2)$$

This equation captures the iterative progression of the radii and offers a concise method for predicting the radii of the composing rings (i.e.,  $r_1, r_2, \dots, r_n$ ) in our tag design. Each succeeding ring radius is essentially determined by multiplying the preceding ring radius with the growth rate and adding the result to the preceding ring radius (e.g.,  $r_2 = r_1(1 + g_r)$ ,  $r_3 = r_2(1 + g_r) = r_1(1 + g_r)(1 + g_r)$ , and so forth). In the example of tag C,  $g_r = 0.208$  was used, which was obtained by substituting  $r_1$ ,  $r_{10}$ , and  $n = 10$  to (2). The complete dimensions of the three tags are provided in Table I when  $t_w = 0.1$  mm was maintained for all the rings.

In Fig. 3(a) and (b), the calculated ring radii of the three tags and their corresponding resonance peaks are shown, respectively. Further, the resultant RCS responses of the tags are provided in Fig. 3(c). Due to the inverse relation between

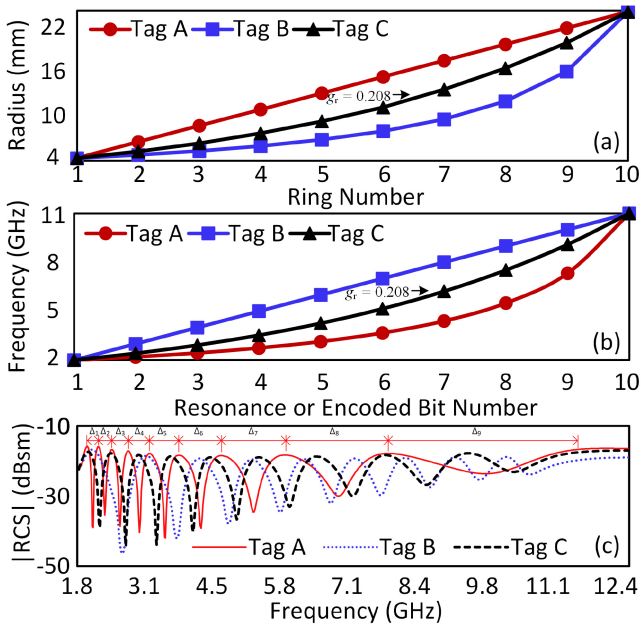


Fig. 3. (a) Calculated rings' radii of the tags shown in Fig. 2 and (b) their associated RCS resonance peaks. (c) Comparison of simulated RCS responses of the tags shown in Fig. 2.

the rings' radii and resonant frequencies described previously, the findings demonstrate ineffective spectrum utilization when employing the conventional constant spacing method. As indicated in Fig. 3(c), particularly in the RCS response of Tag A, it is evident that the distance between the resonance peaks ( $\Delta_1, \Delta_2, \Delta_3 \dots \Delta_9$ ) exponentially widens with increasing frequency. The results also demonstrate the efficacy of the proposed exponential spacing strategy in resolving this issue. Out of the two tags employing the exponential spacing technique, tag B appears to have an RCS response with the most evenly distributed peaks. Such performance is expected since the tag was generated by precisely associating the rings to the evenly spaced frequency points. While remaining open as one of the ways to construct a tag with exponential spacing, this approach can be quite tedious at times, especially when the number of bits is high and fabrication limitations are in place.

For example, in the case of tag B, when a typical minimum track width of 0.3 mm is used, the smallest gap between the rings reaches 0.13 mm, which might be problematic for some PCB manufacturing processes, necessitating further optimization. One solution is to alter the target frequency points for the two inner rings, which, unfortunately, may require tweaking the radii of the other nearby rings. In this regard, the design approach utilized in tag C seems to be more convenient to use. The value of  $g_r$  determined by using the radii of the outer and inner rings can be used as a reference or starting point. This  $g_r$  may well be adjusted further to accommodate a certain degree of spectrum efficiency and different design/fabrication requirements. It should be noted, however, that increasing  $g_r$  beyond this reference point would cause the RCS to fall outside the specified lower frequency limit.

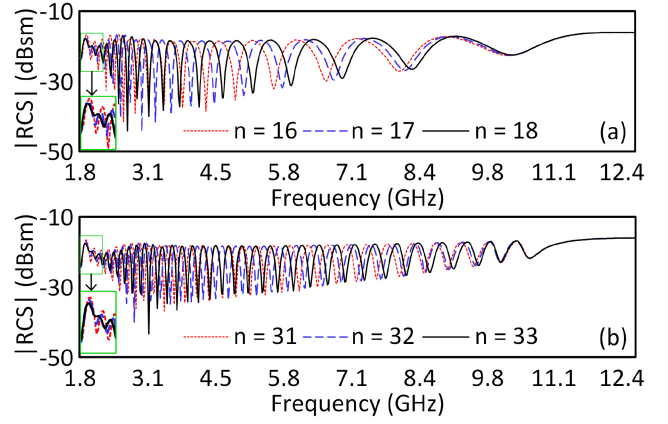


Fig. 4. Simulated RCS responses of tag A (a) and tag C (b) with increasing number of rings. The insets highlight the resonance peaks of the two outermost rings that begin to overlap as the number of rings increases.

### C. Increased Bit Encoding Capacity

The better distribution of the data bits shown in Fig. 3 suggests that not only does the exponential spacing technique result in an easier-to-decode tag, but it also has the potential to have a larger bit capacity than traditionally designed concentric rings tags operating at the same frequency and hence, size. With the exponential spacing technique, there are now more spaces available in the RCS for additional resonances before they become too close to be identified separately.

To examine the impact of the exponential spacing on the encoding capacity, the maximum number of bits that can be encoded by tag C was compared to that of tag A. Keeping the radii of the outer and innermost rings unchanged, the number of rings in between was increased and the RCS response was observed. Our study revealed that, for tag A, when the total number of rings reached 18, the two outermost rings appeared to couple significantly. This was indicated by the fact that their associated resonance peaks were almost merged, thereby preventing further addition of rings. This phenomenon can be seen in Fig. 4(a), which shows the RCS of tag A as the number of rings increases from 16 to 18. In the case of 18 rings, the gap between the two outermost rings was found to be 1.14 mm, which we determined as the minimum spacing necessary for both rings to radiate independently [32]. On the other hand, for tag C, the number of feasible rings before the same coupling phenomenon occurred was higher, i.e., 33 rings. At that point, the gap between the two outermost rings was around 1.14 mm, which is consistent with the case of Tag A with 18 rings. Fig. 4(b) illustrates the RCS of tag C as the total number of rings increasing from 31 to 33, indicating the maximum rings that can be added. These results show an increase of 88.2% in total bit capacity when exponential spacing is implemented.

### D. Nulls for Encoding

Up to this point, the existence of the resonance peak associated with the presence of the ring has been used to encode bit '1'. This implies that the absence of the ring, and hence the resonance peak, has been used to encode bit '0',

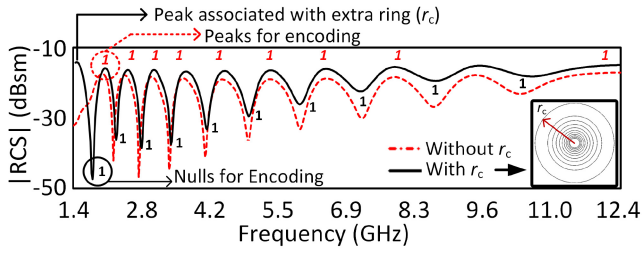


Fig. 5. Simulated RCS of tag C with and without the extra ring ( $r_c$ ). The inset shows tag C after the inclusion of the extra ring ( $r_c = 34.84$  mm). In this case, radii and widths of other rings are maintained as given in Fig. 2(c) and Table I.

as commonly used as the encoding strategy in the literature for concentric rings CRFID tags. However, it is not suited to be implemented in our proposed tag. As indicated in the RCS responses shown in Fig. 3, the last peak associated with the innermost ring is often broadband. Given that this ring is dedicated to sensing in this study, it is difficult to detect the frequency change upon sensing with such a broadband peak. Therefore, instead of the conventional method, we propose associating the ring with its RCS null. Here, the presence and absence of this null would signify logic ‘1’ and ‘0’, respectively. To enable the use of RCS nulls while maintaining the tag’s target  $N$ -bit capacity, an extra ring is added at the outermost edge of the tag. The radius of this ring  $r_c$  also fits into the sequence (2) and can be calculated by treating it as a ring with an index number  $N+2$ . To illustrate this idea, in Fig. 5, the RCS response of tag C before and after the inclusion of the extra ring is shown. With the MSB ( $b_1$ ) started from the first null next to the peak associated with the extra ring  $r_c$ , the RCS clearly illustrates using nulls to represent 10-bit encoded information, as opposed to the scenario when peaks are used.

To further illustrate the encoding procedure proposed in this work, various tag configurations representing various bit combinations were generated. Fig. 6 depicts the tag designs and their associated RCS responses. For instance, by removing rings  $r_9$ ,  $r_5$ ,  $r_4$ , and  $r_1$  from tag C having the extra ring  $r_c$ , the bit combination ‘10111000110’ is obtained (Fig. 6(b)). Consequently, the bit combination ‘1000000011’ (Fig. 6(c)) is generated by removing rings  $r_9 - r_3$ , and the bit combination ‘1001011000’ (Fig. 6(d)) is obtained by eliminating rings  $r_9$ ,  $r_8$ ,  $r_6$ ,  $r_3$ ,  $r_2$ , and  $r_1$ . As can be seen in Fig. 6, with our proposed encoding scheme, bit ‘1’ is identified by the null located prior to the peak generated by the associated ring. In the next subsection, the use of nulls enabling more convenient and accurate sensing potential is illustrated, hence validating the proposed hypothesis.

### E. Sensing

To maintain the simplicity of the tag design, while laying the groundwork for future sensing integration, we have incorporated a potential sensing capability by utilizing one of the constituent rings of the tag. Among the available rings, the innermost ring is a sensible choice since its associated null is located after the identification bits. This implies flexibility

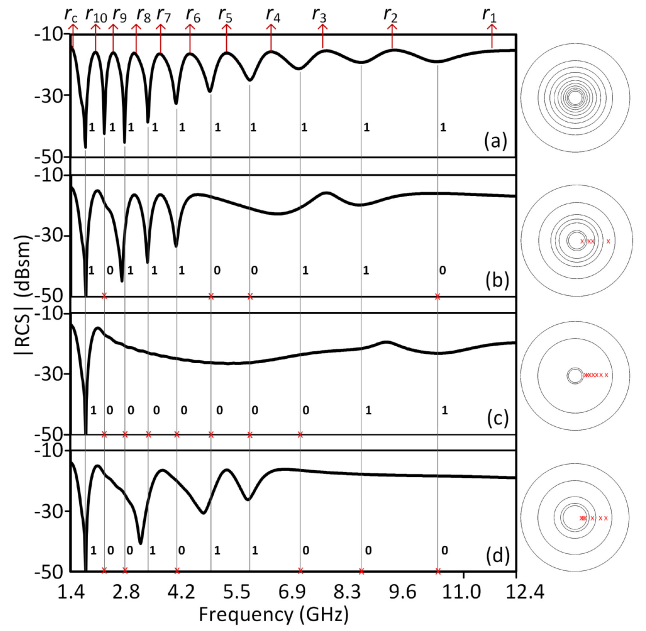


Fig. 6. Different 10-bit combinations generated from tag C with the extra ring ( $r_c = 34.84$  mm): (a) ‘1111111111’, (b) ‘10111000110’, (c) ‘1000000011’, and (d) ‘1001011000’. The radii and widths of other rings are given in Fig. 2(c) and Table I. The tag design for each bit combination is displayed on the right. The ‘x’ symbol denotes the ring removed to encode bit ‘0.’

in terms of the spectrum that can be allocated for sensing, which is controllable through the tag design process. The use of the last null is also useful for minimizing the chance of the identification and sensing data overlapping and hence causing ambiguity in the decoding process. For future sensing implementations, the vision is to incorporate, into interdigital capacitor structures connected to the innermost ring, materials having stimuli-sensitive permittivity such as Kapton, polyvinyl chloride (PVC), polyvinyl alcohol (PVA) [33], vanadium dioxide (VO<sub>2</sub>) [34], and Carboxymethyl cellulose (CMC) [35]. Any change in the relative permittivity of the applied material upon exposure to relevant stimuli (e.g., humidity, temperature, light, to name a few) will result in a corresponding change in the capacitance of the interdigital structures and consequently the ring resonance.

To demonstrate the aforementioned concept, four 0.2 mm gaps were added on the innermost ring of tag C (with the extra outermost ring added), which were then bridged by four capacitors. The quantity and placement of the capacitors, as shown in the inset of Fig. 7(a), were selected to uphold the polarization insensitivity of the tag. It’s noteworthy that this polarization insensitivity is inherently rooted in the radial symmetry properties of circular rings, where a rotation about their center leaves the shape and spatial relationships intact. This geometric characteristic needs to be maintained to ensure that regardless of the tag’s orientation with respect to the reader, the reflection and backscattering profile remain consistent [32]. To showcase the tag’s sensing potential, different capacitance values were applied, and the corresponding RCS responses of the tag are recorded in Fig. 7(a). The results reveal that the frequency of the last null varies with capacitance, confirming

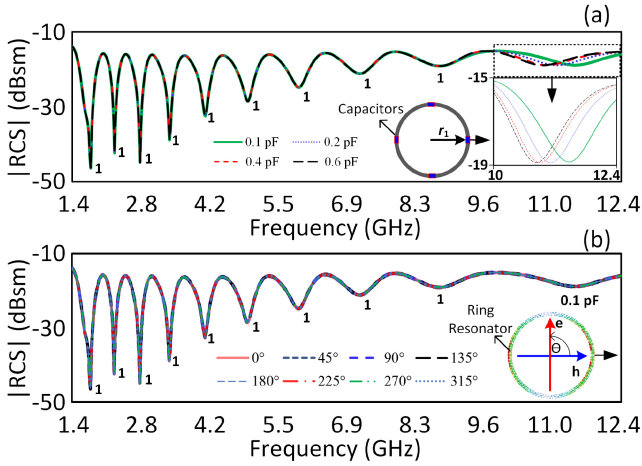


Fig. 7. Simulated RCS of tag C (a) with varying capacitance from 0.1 to 0.6 pF when vertically polarized plane waves were illuminated, (b) with varying polarization of plane waves interrogator (i.e.,  $\theta = 0 - 360^\circ$ ) and 0.1 pF capacitors.

the mechanism explained above. As compared to peaks, the use of nulls allows for a clear observation of this phenomenon. It is also important to note that the variation in the sensing null has an insignificant effect on the other nulls that are used for encoding the identification data. Moreover, as shown in Fig. 7(b), there were no changes observed in the RCS response when the polarization of the plane waves illuminating the tag was altered across a complete range ( $\theta = 0-360^\circ$ ). The consistent tag responses across various polarizations serves as a compelling evidence of the tag's orientation insensitivity.

### F. Synthesis of the Tag

Based on the foregoing numerical findings, practical guidelines for designing the tag are summarized below:

- 1) Determine the target spectrum of the tag and calculate the radii of the outermost ( $r_c$ ) and innermost rings ( $r_1$ ) by substituting into (1) the lower and upper-frequency limits, respectively. For the  $\epsilon_{eff}$ , a number of rings with arbitrary  $r$  but a consistent  $w$  are simulated in both free space and on the target substrate.  $\epsilon_{eff}$  is then approximated by taking the average of  $\epsilon_{eff} = (f_{r,s}/f_{r,b})^2$  [36], where  $f_{r,s}$  is the simulated resonant frequency of the ring in free space, and  $f_{r,b}$  is the resonant frequency of the same ring on the target substrate. This approximation is found to be relatively accurate for the case of a thin ungrounded substrate with printed conductor, placed in air.
- 2) Determine the encoding capacity of the tag ( $N$ ) and calculate the exponential rate  $g_r$  by substituting  $r_c$  and  $r_1$  into (2), noting that  $r_c = r_{N+2}$ .
- 3) Calculate the radii of the remaining rings (i.e.,  $r_2$  to  $r_N$ ) with (2) using the calculated  $g_r$  in step 2.
- 4) Determine the fabrication limitations, i.e., minimum trace width and gaps.
- 5) Set the minimum trace width as  $t_w$ , taking into account the gap limitation.

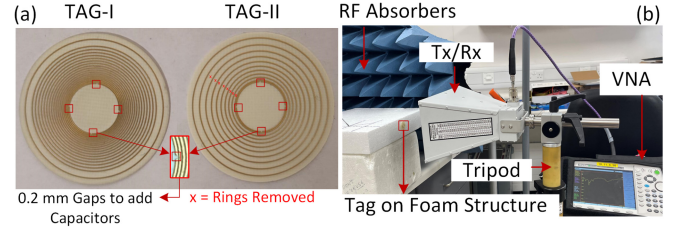


Fig. 8. (a) Fabricated prototypes used to proof the concept: tag I (1111111111111111) and tag II (1010101010101011). Dimensions (all in millimeters) are:  $r_1 = 4, r_2 = 4.2, r_3 = 4.4, r_4 = 4.6, r_5 = 4.9, r_6 = 5.2, r_7 = 5.5, r_8 = 5.8, r_9 = 6.1, r_{10} = 6.4, r_{11} = 6.8, r_{12} = 7.1, r_{13} = 7.5, r_{14} = 7.9, r_{15} = 8.4, r_{16} = 8.8, r_{17} = 9.3, r_{18} = 9.8, r_c = 10.9$ , and  $t_w = 0.1$ . (b) Experimental setup.

- 6) Optimize  $g_r$  as required. Note that increasing  $g_r$  beyond the value derived in step 2 will result in the RCS response exceeding the specified lower frequency limit.

## III. PROOF-OF-CONCEPT EXAMPLE

### A. Design Specifications and Generated Tag Designs

In order to validate further the proposed concept, a number of concentric rings tags are designed and fabricated. The design specifications are given below:

- Upper and lower frequency limits: 3.4 and 9.4 GHz (specified in such a way as to reserve approx. 1.2 GHz bandwidth within the remaining FCC-allowed UWB spectrum for sensing purposes)
- Encoding capacity ( $N$ ): 18 bits (i.e., 17 bits for identification and 1 bit for sensing)
- Substrate: Rogers 4350B,  $h = 0.17$  mm,  $\epsilon_r = 3.6$ , and  $\tan\delta = 0.004$
- Minimum track width and gap: 0.1 mm
- Encoded bits: '1111111111111111' (tag I) and '1010101010101011' (tag II).

Following the guidelines in Section II-F, a tag representing data '1111111111111111' (tag I) was developed. The tag was generated using optimized rates of  $g_r = 0.06$  and  $\epsilon_{eff} = 1.63$  was used in the design process, approximated through simulating six rings having different  $r$ . From tag I, another tag with bit combination '1010101010101011' (tag II) was generated by simply removing from tag I the rings associated with bit '0'. For experimental verification, these tags were fabricated using the specified substrate. The photograph of the fabricated prototypes is shown in Fig. 8(a) and the optimized dimensions can be found in its caption. It is also indicated in Fig. 8(a) the rings which were removed from tag I to develop tag II. To demonstrate the sensing potential, 0201-sized SMD-type capacitors with 0.1, and 0.2 pF were added to the innermost ring of the tags as indicated in Fig. 8(a).

### B. Experimental Characterization and Results

The monostatic approach was chosen for measuring the RCS response of the fabricated tags considering its simplicity [37]. The measurement setup (shown in Fig. 8(b)) consists of a linearly polarized horn antenna (BBHA9120D from Schwarzbeck) connected to a vector network analyzer (VNA) (MS2038C from Anritsu). The measurements were carried

TABLE II  
 COMPARISON WITH STATE-OF-THE-ART CONCENTRIC RINGS/SLOTS-BASED CRFID TAGS

| Antenna     | Frequency (GHz)  | Total Bits | Tag Area (cm <sup>2</sup> ) | Spectral Density (bits/GHz) | Spatial Density (bits/λ <sup>2</sup> ) | Encoding Capacity (bits/λ <sup>2</sup> /GHz) | Sensing    | Shape           |
|-------------|------------------|------------|-----------------------------|-----------------------------|--|--|------------|-----------------|
| [15]        | 5.5 – 9.5        | 5          | 2.25                        | 1.25                        | 35.55                                  | 8.88   | No         | Square          |
| [16]        | 4 – 11           | 10         | 8.25                        | 1.42                        | 19.39                                  | 2.77   | No         | Triangular      |
| [17]        | 3.6 – 15.6       | 10         | 3.64                        | 0.83                        | 26.76                                  | 2.23   | No         | Elliptical      |
| [18]        | 2 – 8            | 10         | 20.25                       | 1.66                        | 17.77                                  | 2.96   | No         | Square          |
| [19]        | 4 – 19           | 15         | 2.40                        | 1                           | 42.53                                  | 2.83   | No         | Pentagonal      |
| [20]        | 4 – 20           | 14         | 2.30                        | 1                           | 38.04                                  | 2.37   | No         | Hexagonal       |
| [25]        | 4.3 – 12         | 9          | 9.6                         | 1.16                        | 12.70                                  | 1.64   | No         | Octagonal       |
| [21]        | 4 – 18           | 12         | 1.72                        | 0.85                        | 51.88                                  | 3.71   | Yes        | Circular        |
| [22]        | 6 – 13           | 8          | 1.91                        | 1.14                        | 41.73                                  | 5.96   | No         | Circular        |
| [23]        | 1 – 3.5          | 5          | 100                         | 2                           | 8.88                                   | 3.55   | No         | Circular        |
| <b>Ours</b> | <b>3.4 – 9.4</b> | <b>18</b>  | <b>3.73</b>                 | <b>3</b>                    | <b>105.92</b>                          | <b>17.65</b>                                 | <b>Yes</b> | <b>Circular</b> |

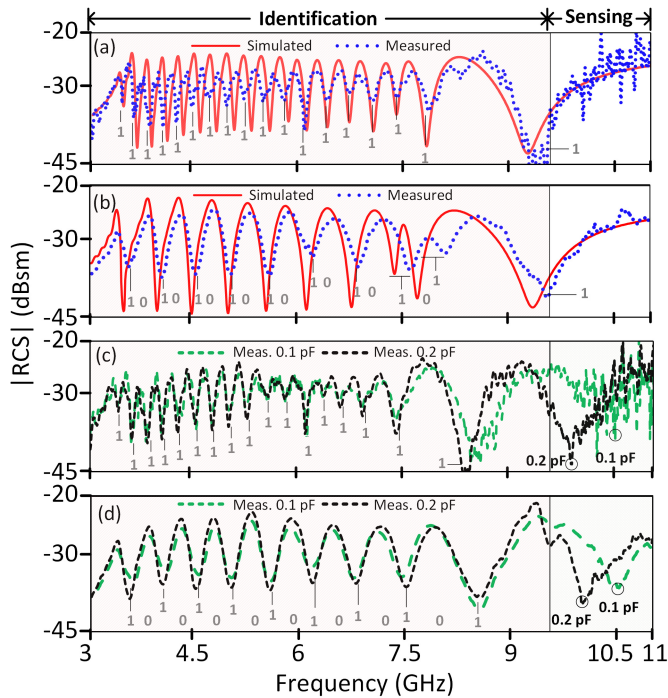


Fig. 9. Simulated and measured RCS responses of the proof-of-concept tags when the gaps in the innermost ring are soldered (no gap case): (a) Tag I, (b) Tag II; and when the gaps are bridged with 0.1 and 0.2 pF capacitors: (c) Tag I, (d) Tag II.

out in a confined laboratory room with RF absorbers put behind the tag to reduce unwanted signal reflections from the surroundings. The tag under test was attached to a supporting foam at a distance of 160 mm from the horn antenna. Using the VNA, a continuous signal from 3 to 11 GHz with 0 dBm of RF power was generated, and the input reflection coefficients were recorded, and the RCS was determined using the method shown in [32].

In Fig. 9, the simulated and measured RCS responses of the developed tags I and II are displayed. The responses of both tags when the gaps in the innermost ring are connected with solder (shown in Fig. 9(a) and (b)) indicate the successful implementation of the tag synthesis process. The

RCS response of tag II, as shown in Fig. 9(b), demonstrates the successful generation of different bit combinations through the removal of appropriate rings. In both tags, the eighteen encoded data bits are well distributed within the specified frequency range, leaving a relatively wide bandwidth to be used by the last null which is earmarked for future sensing applications.

The responses of the tags when the gaps are bridged with different capacitors (see Fig. 9(c) and (d)) offer critical insights into the potential sensing capabilities of our design. These responses illustrate a shift in the frequency position of the last null within the sensing spectrum, correlating with changes in capacitance, validating the foundational concept of tag sensing. In both instances, only measured results are provided for clarity reason. Note also that the shift in the sensing null is accomplished with a negligible influence on the identification nulls, demonstrating the efficacy of the proposed technique in laying the groundwork for a concentric rings-based CRFID tag capable of both identification and prospective sensing functions. Based on our investigations, the discrepancy in the measured results is attributed to fabrication inaccuracies, specifically the manual soldering used to bridge the gaps in the innermost ring. The presence of excess solder tin at locations where the induced currents on the innermost ring are the maximum results in additional parasitic (capacitive and inductive) effects [38], [39] on the tag. Such defects have a substantial impact on the overall performance of tag I, which consists of tightly-arranged resonators. When there are wider gaps between the rings, as in tag II, such parasitic effects are less significant. Utilizing an industry-standard manufacturing/assembly process can help mitigate this issue.

In Table II, the proposed CRFID tag is compared to state-of-the-art concentric rings/slots-based CRFID tags. The comparison is restricted to works that employ one ring/slot for one-bit data encoding and provide experimental validation. For a comprehensive comparison of the proposed design methodology we have utilized three relevant metrics, namely, spectral capacity, spatial density, and encoding capacity, as given in [40].

Spectral capacity (bits/GHz) provides the efficiency of data encoding within a given bandwidth. It is calculated by dividing the number of bits encoded to the bandwidth utilized in GHz, offering insights into the information density achievable within the frequency range. On the other hand, spatial density, measured in bits per square wavelengths ( $\text{bits}/\lambda^2$ ), indicates the amount of data accommodated within a specified tag area, where  $\lambda$  represents the wavelength at the tag's center frequency. This metric is computed by dividing the total number of bits by the surface area of the tag in square wavelengths, allowing an assessment of information concentration in a spatial context. Furthermore, encoding capacity, expressed in bits per lambda squared per GHz ( $\text{bits}/\lambda^2/\text{GHz}$ ), showcases the encoding capability in relation to both tag area and bandwidth. It is derived by dividing the spatial density to the operating bandwidth in GHz. Such a comparison thus involves utilizing the relative dimensions of the tag area (in wavelength-squared) in order to correctly compare tags designed for different operating bandwidths [40]. These additional metrics provides a more comprehensive understanding of our tag's performance. The results of this comparative analysis are quite revealing. Our proof-of-concept tag, which is a direct application of our proposed design methodology, demonstrates superior performance across all three metrics of spectral capacity, spatial density, and encoding capacity when compared to the designs presented in other referenced papers. In addition, our tag uniquely combines these high-performance metrics with the potential for simultaneous data encoding and sensing.

The achieved results suggest that a larger bit capacity can be achieved if the proposed technique is applied to tags employing hybrid encoding techniques in which a single resonator is used for multiple-bit encoding [32], [41].

#### IV. CONCLUSION

In this work, we have successfully demonstrated a novel class of concentric-rings chipless tags, employing a combination of exponential spacing and null encoding techniques. This design marks a departure from traditional concentric rings tags, offering a platform that is not only suitable for carrying identification data but also prepared for future integration of sensing capabilities. Our approach optimally distributes encoded bits within the target spectrum, facilitating the decoding process and enabling the design of a simpler reader. Such a feature also allows for a higher capacity tag, especially when compared to conventionally-designed concentric tags of the same size. The proof-of-concept 18-bit tags developed in this study validate our approach, with the eighteen nulls representing the encoded information effectively distributed between 3.4 and 9.4 GHz. The design strategically allocates the last null to utilize the remaining FCC UWB band, anticipating high-resolution sensing capabilities without impinging on the identification nulls.

The advancements presented in this paper open avenues for a wide range of applications, including enhanced inventory management, anti-counterfeiting measures, and real-time environmental monitoring, with potential impacts across various

sectors such as retail, logistics, and agriculture. However, we recognize that our current demonstration, which relies on controlled experiments using capacitors, represents an initial step. This method serves to demonstrate the foundational functionality of our design but may not fully encapsulate the complexities and variabilities of the real sensing implementations. In light of this, our future research is directed toward integrating actual stimuli-sensitive materials into the tag designs. These materials, potentially deposited on interdigital structures connected to the sensing ring, will facilitate the direct sensing of environmental parameters like temperature and humidity, leading to a more realistic and robust implementation of our tag design. Furthermore, we plan to test these tags in more dynamic and realistic scenarios, taking into account diverse platform shapes, varying read ranges, orientation angles, potential interferences, and noise. An additional goal is to explore the use of machine-learning algorithms for the effective extraction of encoded identification and sensing data. Such advancements will not only enhance the functionality of our tags but also expand their applicability in practical, real-world settings. This forward-looking approach underscores our commitment to evolving the field of chipless RFID technology, bridging the gap between current capabilities and future possibilities.

#### REFERENCES

- [1] O. Rance, R. Siragusa, P. Lemaitre-Auger, and E. Perret, "Toward RCS magnitude level coding for chipless RFID," *IEEE Trans. Microw. Theory Techn.*, vol. 64, no. 7, pp. 2315–2325, Jul. 2016.
- [2] N. Rather, R. B. Simorangkir, J. Buckley, B. O'Flynn, and S. Tedesco, "Evaluation of machine learning models for a chipless RFID sensor tag," in *Proc. 17th Eur. Conf. Antennas Propag. (EuCAP)*, 2023, pp. 1–5.
- [3] K. Brinker and R. Zoughi, "A review of chipless RFID measurement methods, response detection approaches, and decoding techniques," *IEEE Open J. Instrum. Meas.*, vol. 1, pp. 1–31, Aug. 2022, doi: [10.1109/OJIM.2022.3196746](https://doi.org/10.1109/OJIM.2022.3196746).
- [4] M. Polivka and M. Svanda, "High encoding capacity chipless RFID tag," in *Proc. 17th Eur. Conf. Antennas Propag. (EuCAP)*, 2023, pp. 1–4.
- [5] F. Babaecian, J. Feng, and N. Karmakar, "Realisation of a high spectral efficient chipless RFID tag using hairpin resonators," in *Proc. IEEE Asia Pac. Microw. Conf. (APMC)*, 2019, pp. 114–116.
- [6] M. Noman, U. A. Haider, H. Ullah, A. M. Hashmi, and F. A. Tahir, "Realization of chipless RFID tags via systematic loading of square split ring with circular slots," *IEEE J. Radio Freq. Identification*, vol. 6, pp. 671–679, Oct. 2022, doi: [10.1109/JRFID.2022.3211301](https://doi.org/10.1109/JRFID.2022.3211301).
- [7] S. Genovesi et al., "Enhanced chipless RFID tags for sensors design," in *Proc. IEEE Int. Symp. Antennas Propag. (APSURSI)*, 2016, pp. 1275–1276.
- [8] M. Forouzandeh and N. C. Karmakar, "Chipless RFID tags and sensors: A review on time-domain techniques," *Wireless Power Transfer*, vol. 2, no. 2, pp. 62–77, 2015.
- [9] N. C. Karmakar, E. M. Amin, and J. K. Saha, *Chipless RFID Sensors*, Hoboken, NJ, USA: Wiley, Inc., 2016.
- [10] A. Vena, E. Perret, and S. Tedjini, "A fully printable chipless RFID tag with detuning correction technique," *IEEE Microw. Compon. Lett.*, vol. 22, no. 4, pp. 209–211, Apr. 2012.
- [11] M. Mumtaz, S. F. Amber, A. Ejaz, A. Habib, S. I. Jafri, and Y. Amin, "Design and analysis of C shaped chipless RFID tag," in *Proc. Int. Symp. Wireless Syst. Netw. (ISWSN)*, 2017, pp. 1–5.
- [12] A. Vena, E. Perret, S. Tedjini, D. Kaddour, A. Potie, and T. Barron, "A compact chipless RFID tag with environment sensing capability," in *Proc. IEEE/MTT-S Int. Microw. Symp. Dig.*, 2012, pp. 1–3.
- [13] A. Habib, A. Mirza, M. Y. Umair, M. N. Salimi, S. Ahmed, and Y. Amin, "Data dense chipless RFID tag with efficient band utilization," *AEU-Int. J. Electron. Commun.*, vol. 152, Jul. 2022, Art. no. 154220.
- [14] N. Javed, M. Azam, and Y. Amin, "Chipless RFID multisensor for temperature sensing and crack monitoring in an IoT environment," *IEEE Sens. Lett.*, vol. 5, no. 6, pp. 1–4, Jun. 2021.

- [15] N. Chen, Y. Shen, G. Dong, and S. Hu, "Compact scalable modeling of chipless RFID tag based on high-impedance surface," *IEEE Trans. Electron Devices*, vol. 66, no. 1, pp. 200–206, Jan. 2018.
- [16] S. Rauf, M. A. Riaz, H. Shahid, M. S. Iqbal, Y. Amin, and H. Tenhunen, "Triangular loop resonator based compact chipless RFID tag," *IEICE Electron. Exp.*, vol. 14, no. 4, 2017, Art. no. 20161262.
- [17] I. Jabeen, A. Ejaz, A. Akram, Y. Amin, J. Loo, and H. Tenhunen, "Elliptical slot based polarization insensitive compact and flexible chipless RFID tag," *Int. J. RF Microw. Comput. Aided Eng.*, vol. 29, no. 11, 2019, Art. no. e21734.
- [18] F. Costa, S. Genovesi, and A. Monorchio, "A chipless RFID based on multiresonant high-impedance surfaces," *IEEE Trans. Microw. Theory Techn.*, vol. 61, no. 1, pp. 146–153, Jan. 2012.
- [19] T. Bibi, A. T. Khan, Y. Amin, and S. Ahmed, "RFID in IoT, miniaturized pentagonal slot-based data dense chipless RFID tag for IoT applications," *Arabian J. Sci. Eng.*, vol. 47, pp. 1147–1157, Feb. 2022.
- [20] M. S. Iqbal, H. Shahid, M. A. Riaz, S. Rauf, Y. Amin, and H. Tenhunen, "FSS inspired polarization insensitive chipless RFID tag," *IEICE Electron. Exp.*, vol. 14, no. 10, 2017, Art. no. 20170243.
- [21] N. Javed, M. A. Azam, I. Qazi, Y. Amin, and H. Tenhunen, "A novel multi-parameter chipless RFID sensor for green networks," *AEU Int. J. Electron. Commun.*, vol. 128, Jan. 2021, Art. no. 153512.
- [22] M. A. Islam, Y. Yap, N. C. Karmakar, and A. Azad, "Compact printable orientation independent chipless RFID tag," *Progress Electrom. Res. C*, vol. 33, pp. 55–66, Sep. 2012.
- [23] M. Anuar et al., "Design chipless textile tag for RFID application," *J. Phys., Conf. Series*, vol. 1339, no. 1, 2019, Art. no. 012028. [Online]. Available: <https://iopscience.iop.org/article/10.1088/1742-6596/1339/1/012028/meta>
- [24] A. Fawky, M. Khaliel, A. El-Awamry, and T. Kaiser, "Frequency coded chipless RFID tag localization using multiple antennas," in *Proc. 11th Eur. Conf. Antennas Propag. (EUCAP)*, 2017, pp. 2075–2079.
- [25] I. Jabeen, A. Ejaz, S. M. Kabir, A. Akram, Y. Amin, and H. Tenhunen, "Octagonal shaped flexible chipless RFID tag for Internet of Things," in *Proc. Int. Conf. Elec., Commun., Comput. Eng. (ICECCE)*, 2019, pp. 1–4.
- [26] C. A. Balanis, "Loop antennas," in *Antenna Theory*, 3rd ed. Hoboken, NJ, USA: Wiley Inc., 2005, pp. 272–273, ch. 5.
- [27] G. Breed, "A summary of FCC rules for ultra wideband communications," *High Freq. Electron.*, vol. 4, no. 1, pp. 42–44, 2005.
- [28] Y. Zhang, Z. Guo, W. Wang, S. He, T. Lee, and M. Loew, "A comparison of the wavelet and short-time fourier transforms for doppler spectral analysis," *Med. Eng. Phys.*, vol. 25, no. 7, pp. 547–557, 2003.
- [29] R.-E. Azim, N. Karmakar, and E. Amin, "Short time fourier transform (STFT) for collision detection in chipless RFID systems," in *Proc. Int. Symp. Antennas Propag. (ISAP)*, 2015, pp. 1–4.
- [30] G. Khadka, M. A. Bibile, L. M. Arjomandi, and N. C. Karmakar, "Analysis of artifacts on chipless RFID backscatter tag signals for real world implementation," *IEEE Access*, vol. 7, pp. 66821–66831, 2019.
- [31] N. Rather, J. Buckley, B. O'Flynn, and M. Pigeon, "A novel RCS based CRFID tag design," in *Proc. 16th Eur. Conf. Antennas Propag. (EuCAP)*, 2022, pp. 1–5.
- [32] A. Vena, E. Perret, and S. Tedjini, "High-capacity chipless RFID tag insensitive to the polarization," *IEEE Trans. Antennas Propag.*, vol. 60, no. 10, pp. 4509–4515, Oct. 2012.
- [33] N. C. Karmakar, E. M. Amin, and J. K. Saha, "Smart materials for chipless RFID sensors," in *Chipless RFID Sensors*. Hoboken, NJ, USA: Wiley Inc., 2016, pp. 69–88, ch. 4.
- [34] D. E. Anagnostou, D. Torres, T. S. Teeslink, and N. Sepulveda, "Vanadium dioxide for reconfigurable antennas and microwave devices: Enabling RF reconfigurability through smart materials," *IEEE Antennas Propag. Mag.*, vol. 62, no. 3, pp. 58–73, Jun. 2020.
- [35] G. A. Eyebe, B. Bideau, N. Boubekeur, R. Loranger, and F. Domingue, "Environmentally-friendly cellulose nanofibre sheets for humidity sensing in microwave frequencies," *Sens. Actuators B, Chem.*, vol. 245, pp. 484–492, Jun. 2017.
- [36] Z. Živković, A. Šarolić, and V. Roje, "Effects of effective dielectric constant of printed short dipoles in electric field probes," in *Proc. 10th Int. Symp. Electromagn. Compat.*, 2011, pp. 73–78.
- [37] *IEEE Recommended Practice for Radar Cross-Section Test Procedures*, Standard 1502-2020, (Revision of IEEE Std 1502-2007), 2020.
- [38] Z. Wang, L. Wang, K. Yu, S. Liu, and C. Wang, "Equivalent circuit based performance coupling analysis method for lead wire interconnection with defects," *Electronics*, vol. 9, no. 4, p. 642, 2020.
- [39] S. Luo, M. Thorburn, and V. Tripathi, "Modelling of multiple coupled concentric open and closed microstrip ring structure," in *IEEE Proc. H (Microw., Antennas Propag.)*, vol. 138, no. 6, pp. 573–576, 1991.
- [40] M. Svanda, M. Polivka, J. Havlicek, J. Machac, and D. H. Werner, "Platform tolerant, high encoding capacity dipole array-plate chipless RFID tags," *IEEE Access*, vol. 7, pp. 138707–138720, 2019.
- [41] M. E. B. Jalil et al., "High capacity and miniaturized flexible chipless RFID tag using modified complementary split ring resonator," *IEEE Access*, vol. 9, pp. 33929–33943, 2021.